Optics Communications 355 (2015) 331–336

Contents lists available at ScienceDirect

Optics Communications

journal homepage: www.elsevier.com/locate/optcom

Radius vertical graded nanoscale interlaced-coupled photonic crystal sensors array

Pan Zhang, Huiping Tian*, Daquan Yang, Qi Liu, Jian Zhou, Lijun Huang, Yuefeng Ji

The State Key Laboratory of Information Photonics and Optical Communications, School of Information and Telecommunication Engineering, Beijing University of Posts and Telecommunications, Beijing 100876, China

ARTICLE INFO

Article history:
Received 23 January 2015
Received in revised form
23 April 2015
Accepted 18 May 2015
Available online 21 May 2015

Keywords:
Photonic crystal sensors array
Resonant cavity
Crosstalk
Photonic crystal waveguide
Refractive index sensitivity

ABSTRACT

A radius vertical graded photonic crystal sensors array based on a monolithic substrate is proposed, which is potentially to be used as label-free detection in aqueous environments. The sensors array device consists of five resonant cavities including three H1 cavities and two L2 cavities which are interlaced-coupled to a radius vertical graded single photonic crystal line defect waveguide (W1). Each resonator has a different resonant wavelength dip which can shift independently with crosstalk lower than −13 dB in response to the refractive index change of air holes around every cavity. With three-dimensional finite-difference time-domain (3D-FDTD) method, simulation results demonstrate that the quality factors of microcavities are over 10^4. Besides, the refractive index sensitivity is 100 nm/RIU with the detection limit approximately of 5.63×10^{-4}. Meanwhile, the radius vertical graded photonic crystal with more interlaced cavities is more suited to ultracompact optical monolithic integration.

1. Introduction

Photonic crystal (PhC) sensor is widely used for lab-on-a-chip applications due to its advantages including ultracompact size, high sensitivity and more suitable for monolithic integration. During the last decades, many structures have been proposed to realize photonic crystal sensors, such as microcavities [1,2], slot waveguides [3,4], resonant rings and disks [5], heterostructures [6,7], and so on. These numerous different architectures have been developed in nearly all sensing detection cases, like stress sensing, refractive index sensing, temperature sensing, and biochemical sensing [8–11]. The sensing detection mechanism relies on the shift of the resonant wavelength peak due to the change in refractive index.

With the extensive research about photonic crystal sensors, photonic crystal sensor arrays have attracted considerable interest for subminiature and integrated sensing. Sensor arrays could combine the high quality factor, high sensitivity with the ability to multiplex multiple detection sites. Since Mandal et al. firstly proposed the nanoscale optofluidic sensor arrays based on silicon waveguide with 1D (one dimensional) photonic crystal microcavity [12], many researchers have focused on the study of sensor arrays. Examples of such research include that of Gylfason who demonstrated on-chip temperature compensation in an integrated slot-waveguide ring resonator refractive index sensor array [13], Iqbal et al. who designed label-free biosensor arrays based on silicon ring resonators and high-speed optical scanning instrumentation [14], and Pal et al. who proposed a multiple nanocavity coupled device for error-corrected optical biosensing [15]. All these devices are applied as sensor arrays for accurately sensing detections but not suitable for compact optical integration.

The graded photonic crystal is an interesting topic in recent years. Works have mainly focused on the electromagnetic waves which propagate and transform along the graded structure. Due to its ability of efficiently controlling the light propagation, the graded photonic crystal has been successfully applied as light bending and demultiplexer [16–18]. What's more, since the electromagnetic waves in the graded structure have different light properties, it has also been used as lens in practical applications [19,20]. According to the advantages of radius-graded structure, if we combine it with cavity multiplex as photonic crystal sensors array, the sensing scale could be smaller than that proposed in [12,15].

In a previous work [21], we have proposed a photonic crystal sensors array with radius grading along waveguide direction, which consisted of four resonant cavities. In this paper, we describe a new photonic crystal sensors array based on the radius vertical graded structure. This design contains five resonant cavities (three H1 cavities and two L2 cavities) interlaced-coupled along W1 waveguide, which makes it more suitable to ultracompact optical monolithic integration. FDTD (finite difference

* Correspondence to: Beijing University of Posts and Telecommunications, P.O. BOX 90, #10 Xitucheng, Road Haidian District, Beijing 100876, China.
E-mail address: hptian@bupt.edu.cn (H. Tian).

http://dx.doi.org/10.1016/j.optcom.2015.05.037
0030-4018/

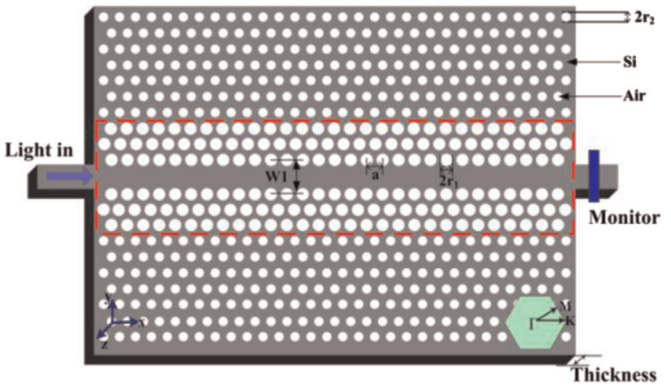

Fig. 1. 3D illustration of the radius vertical graded photonic crystal with a line defect waveguide, where $a=416$ nm, $T=0.58a$, $r_1=0.32a$, and $r_2=0.28a$. (For interpretation of the references to color in this figure, the reader is referred to the web version of this article.)

detection. In addition, the resonant wavelength shifts linearly with refractive index change, and the sensitivity of the sensor array is 100 nm/RIU. The detection limit of refractive index changes (DL) determined by resonant wavelength, sensitivity and quality factor is about 5.63×10^{-4}. The footprint of our design is only $12.48\times7.20\ \mu m^2$ which is much smaller than $60\times60\ \mu m^2$ proposed in [22]. It is essential for photonic crystal sensors array application for the compact optical integrated circuit in the future.

2. Design of the photonic crystal sensors array based on radius-graded structure

2.1. Side-coupled resonant cavity design

Fig. 1 shows a 3D illustration of our radius vertical graded photonic crystal waveguide structure design which is based on

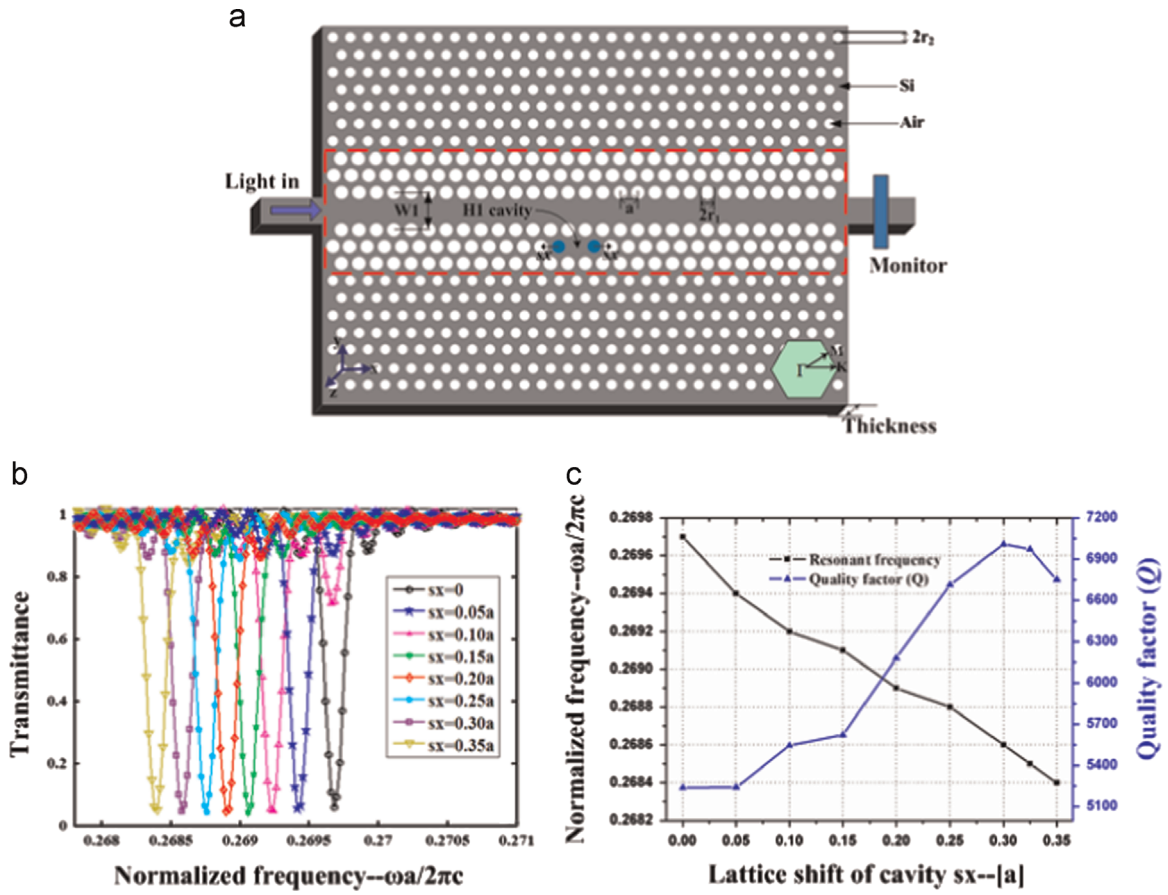

Fig. 2. (a) Schematic diagram of the radius vertical graded PhC with H1 cavity; (b) transmission spectra of TE-like polarized light in resonant cavity with different shifts ranging from $sx=0$ to $sx=0.35a$; and (c) results of FDTD calculations showing the resonant frequencies and quality factors on different sx.

time domain) method is a numerical analysis method that directly uses Maxwell's equations to simulate the electromagnetic field. FDTD has a wide range of applications. One can use FDTD to simulate performances of various complex electromagnetic structures, including scattering, radiation, transmission, absorption, and so on. With the development of time step, FDTD can directly simulate the transmission of electromagnetic wave and its interaction with the object so that the researchers can get a clear description. Through the 3D-FDTD simulation of our designed structure, we can observe that each cavity has much higher transmittance and Q factor. The dip is down to 0.03 and the Q factor is up to 10^4, which is beneficial for accurately sensing triangular lattice and hole-array. It is constructed in a silicon slab ($n_{si}=3.48$) by arranging a triangular lattice of air holes, where the central row of air holes is removed in order to form a line defect waveguide (W1). In this paper, the preliminary analysis of structures has been performed by using the commercial FDTD software RSoft to calculate their photonic band structure and transmission spectra [2]. For improving the accuracy in the simulation, FDTD analysis of photonic crystal structure is carried out with a grid size of $a/100$ and time step of $0.025a/c$, where a is the lattice constant. All the simulations are carried out with the same grid size and time step for future comparable results. The boundary conditions at the spatial edges of the computational domain must be carefully

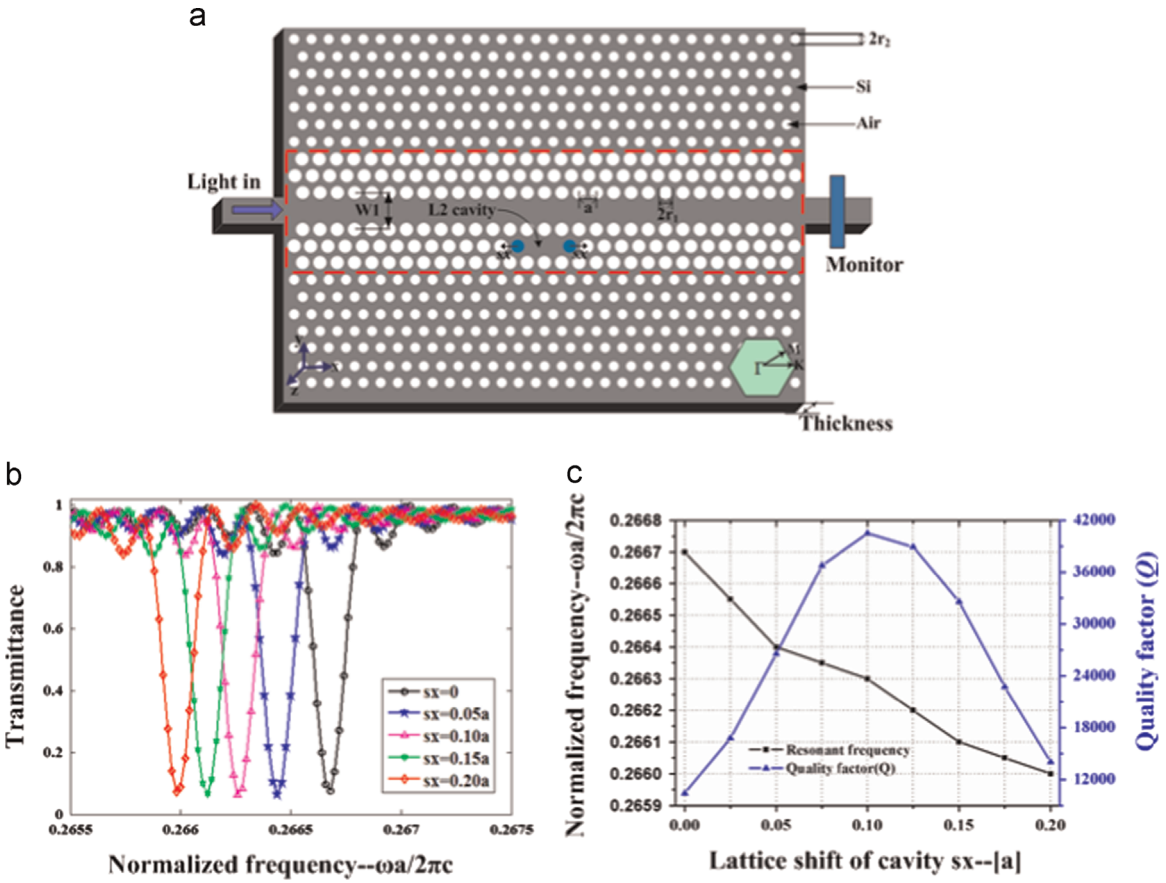

Fig. 3. (a) Schematic diagram of the radius vertical graded PhC with L2 cavity; (b) transmission spectra of TE-like polarized light in resonant cavity with different shifts ranging from $sx=0$ to $sx=0.2a$; and (c) results of FDTD calculations showing the resonant frequencies and quality factors on different sx.

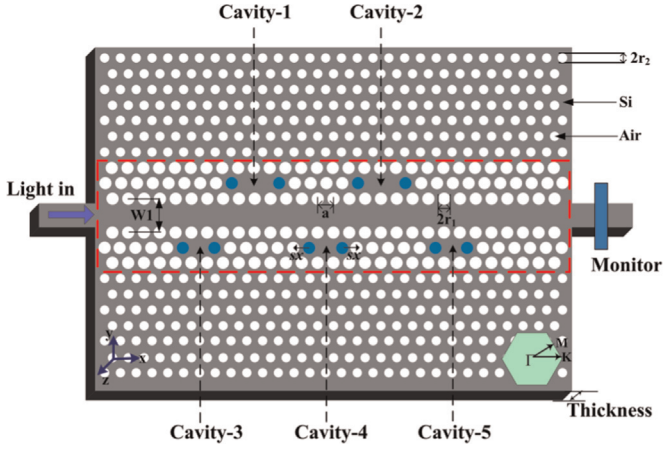

Fig. 4. 3D illustration of radius vertical graded photonic crystal sensors array with five interlaced microcavities (two L2 cavities and three H1 cavities), where $a=416$ nm, $T=0.58a$, $r_1=0.32a$, and $r_2=0.28a$.

considered. The simulation area in our paper is surrounded by one-spatial unit thick perfectly matched layer (PML), in which both electric and magnetic conductivities are introduced in such a way that the wave impedance remains constant, absorbing the energy without inducing reflections.

As shown in Fig. 1, the lattice constant in the photonic crystal is $a=416$ nm and the thickness is $T=0.58a=240$ nm. In order to introduce radius vertical graded structure based on photonic crystal slab, we set the air holes along vertical direction with two different radius parameters (r_1 and r_2). With careful design about the radius vertical graded photonic crystal, the holes in PhC are set as $r_1=0.32a$ and $r_2=0.28a$, respectively. Using graded photonic crystal structure, we can add more resonant cavities interlaced-coupled to the waveguide.

We then research the light properties of different side-coupled resonant cavities based on the radius vertical graded structure to design photonic crystal sensors array. The design of H1 cavity coupled to the radius vertical graded photonic crystal waveguide is shown in Fig. 2(a).

The H1 resonant cavity is optimized by using 3D-FDTD method for a Si device layer. The basic device parameters are the same as that presented in Fig. 1. We increase the Q-factor of H1 cavity by slightly shifting the two blue air holes (in the horizontal direction) outwards in the opposite direction (sx). The air holes shift sx is varied from 0 to a maximum shift of $0.35a$ in the interval of $0.05a$. An air hole moving of $0.3a$ results in the highest Q factor of 7007. The transmission spectra of TE polarized lightwave with different lattice shifts is shown in Fig. 2(b). Fig. 2(c) demonstrates the Q factors and resonant frequencies in terms of the lattice shift sx. The simulation results show that the resonant frequency moves towards lower with the shift sx increasing, due to the increase in high-dielectric material in the cavity region. On the other hand, the Q factor increases when sx increases, but eventually it reaches a maximum and decreases again.

Another side-coupled cavity (L2 cavity) for radius-graded photonic crystal sensors array design is presented in Fig. 3(a). The resonant frequency and Q factor are also simulated according to the shifts of the air holes around the cavity, which is illustrated in Fig. 3(c). Desired results are observed, and the highest Q factor is 40,518 at $\omega=0.2663(2\pi c/a)$ with a lattice shift of $0.1a$. The transmission spectra with different lattice shifts ranging from $sx=0$ to

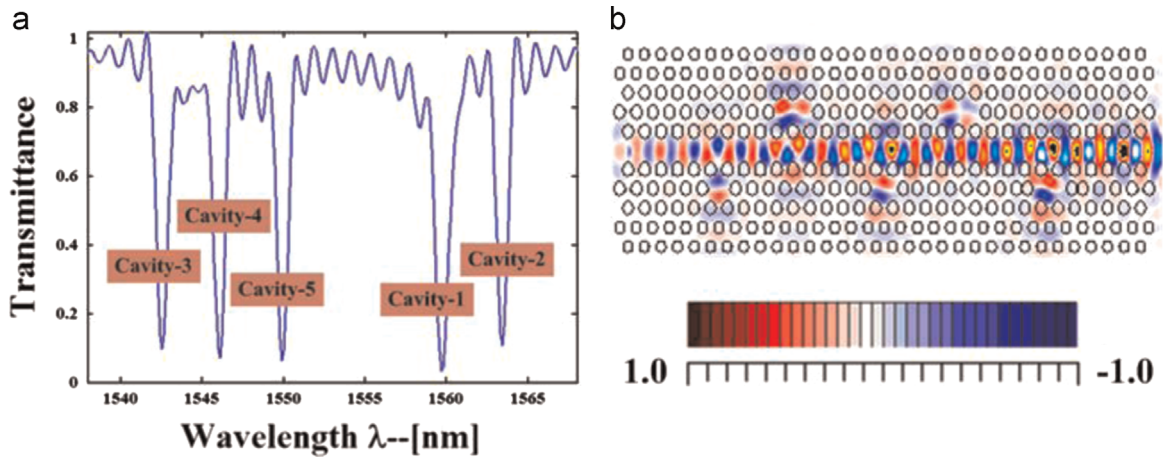

Fig. 5. (a) The transmission spectra of radius vertical graded photonic crystal sensors array with five interlaced microcavities and (b) steady electric field distribution for the structure pictured in Fig. 5.

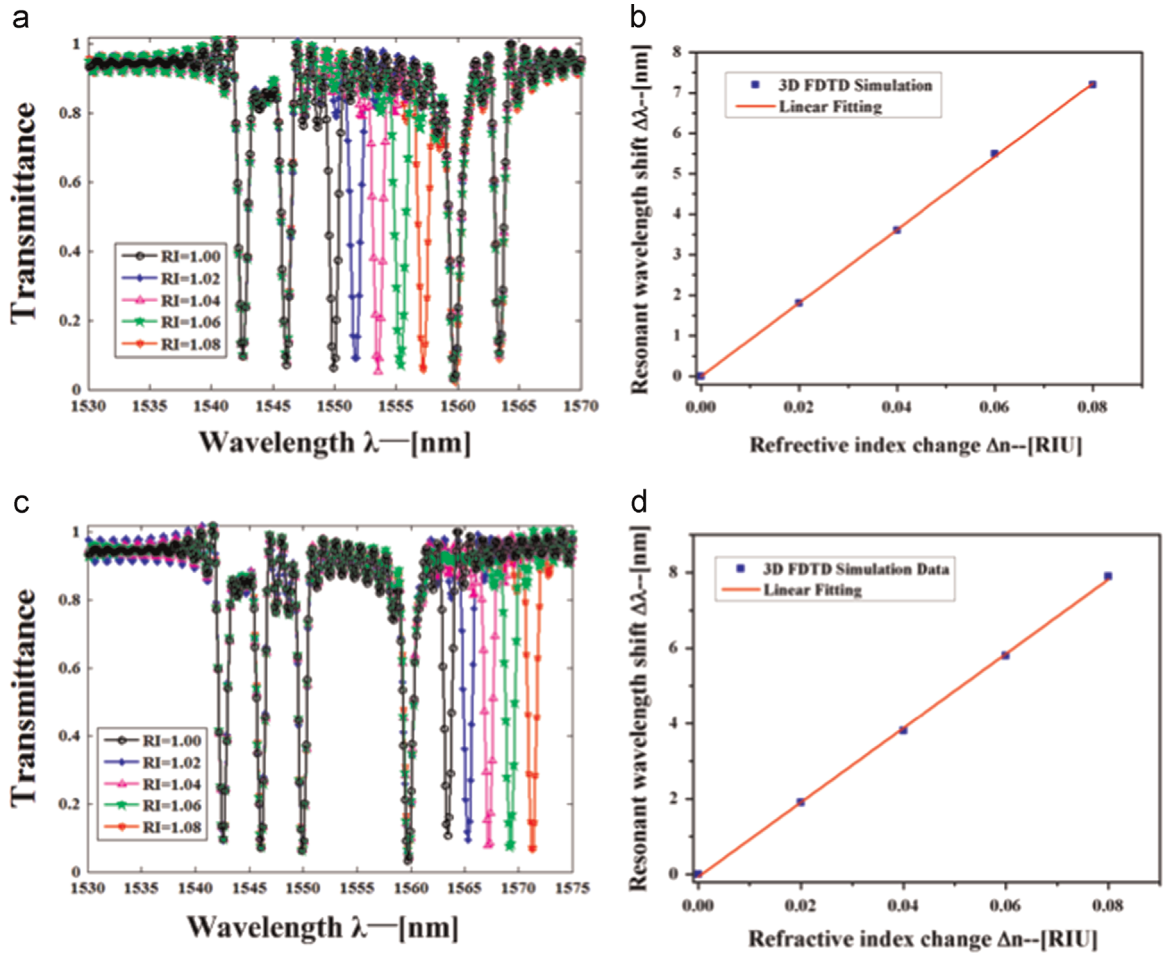

Fig. 6. Normalized transmission spectra observed when five sensors are set interlaced to W1 waveguide and one of them is subjected to the changes in refractive index. (a) H1-cavity-5; (c) L2-cavity-2. The corresponding relationship between refractive index change and resonant wavelength shift for are separately shown in (b) and (d).

$sx=0.2a$ are performed in Fig. 3(b).

Considering the above discussions about two kinds of resonant cavities (H1 and L2 cavity), we can see that H1 cavity has smaller footprint and L2 cavity has higher Q factor. When we multiplex the two different resonators interlaced-coupled to the W1 waveguide, the device would have compact scale and high quality factor which are better than the single cavity multiplex in photonic crystal sensors array.

2.2. Radius vertical graded photonic crystal sensors array design

Through the design and discussion of two kinds of side-coupled resonant cavity (H1 and L2 cavity) based on the radius-graded photonic crystal in above sections, the photonic crystal sensors array is made up of five interlaced microcavities including three H1 cavities and two L2 cavities, which is under the tradeoff between Q factor and compactness. Fig. 4 shows the 3D illustration of

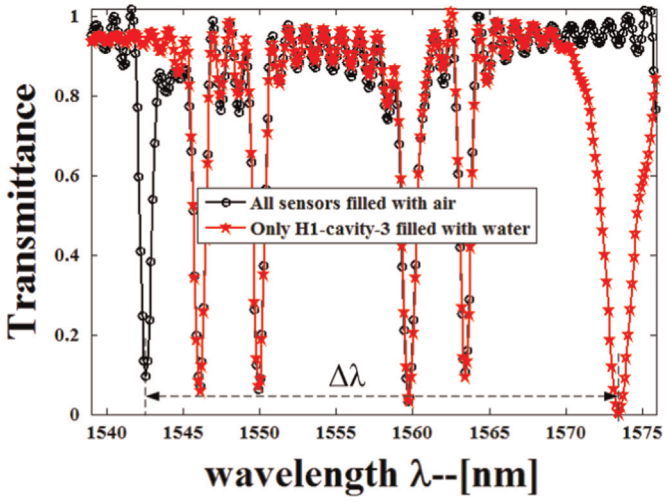

Fig. 7. The output spectra of a PhC sensors array with five resonators under two different conditions, the black line represents all sensors are in air situation, while the red line is the case when one of sensors is subjected with water. (For interpretation of the references to color in this figure legend, the reader is referred to the web version of this article.)

radius vertical graded photonic crystal sensors array with five interlaced microcavities. The cavity-1 and cavity-2 are L2 cavities with different shifts while cavity-3 to cavity-5 are H1 resonant cavities. The parameters of each resonator in PhC sensors array are as follows: L2-cavity-1: $sx=0$; L2-cavity-2: $sx=0.15a$; H1-cavity-3: $sx=0$; H1-cavity-4: $sx=0.15a$; H1-cavity-5: $sx=0.35a$. When five sensors are set interlaced to the W1 waveguide with a triangular lattice of air holes on silicon slab, the transmission spectra of the sensors array exhibits five dips. The sensing property is explained specifically in the next section.

3. Simulation results and discussion

It is essential to note that the resonant wavelength dips in photonic crystal sensors array should be independent of each other, and a shift in one of them does not disturb the others. It is the basic requirement for more complex optical integrated circuits and integrated optical devices. Fig. 5(a) demonstrates the output spectra of radius vertical graded photonic crystal sensors array which has been pictured in Fig. 4. There are five resonant wavelength dips around the 1550 nm corresponding to five interlaced microcavities. As can be seen, the five resonant wavelengths have the appropriate intervals which can be separated clearly. What's more, the resonant dip could be dropped down to ~0.03 and it is much better than in the previous work [21]. The steady electric field distribution of the PhC sensors array is shown in Fig. 5(b). We can see that the light is confined strongly in the five resonant cavities, and the leakage of light becomes small. In addition, the strong light confinement in resonators means high Q factors which can be significantly used for optimizing the device geometry to allow an even larger degree of multiplexing.

Based on the above optimal design, the multiplexing is quite straightforward (by setting five resonant cavities interlaced-coupled to W1 waveguide). To verify the performance of the sensors in series, each sensor is independently subjected to the changes in refractive index. Fig. 6 shows the composed transmission spectra of PhC sensors array when one sensor is under different refractive index conditions while others keep constant. As can be seen from Fig. 6(a), H1-cavity-5 is under variation in refractive index (RI-1, RI-2, RI-3, RI-4, and RI-5, respectively). The shift only exists in one dip and other dips remain completely unchanged. The same phenomenon occurs when only L2-cavity-2 is with refractive index changing, which is demonstrated in Fig. 6(c).

In order to quantitatively analyze the refractive index sensitivity of radius vertical graded sensors array, we observe the resonant wavelength shifts as a function of the change in refractive index. The refractive index sensitivity can be expressed as [21,23]

$$S = \frac{\Delta\lambda}{\Delta n} \tag{1}$$

$\Delta\lambda$ means the shift of resonant wavelength, and Δn represents the change in refractive index.

Therefore, the calculated refractive index sensitivity of the radius vertical graded PhC sensors array is equal to 100 nm/RIU (RIU=refractive index unit) and 90 nm/RIU as shown in Fig. 6 (b) and (d), respectively. When introduced in sensors array in our paper, the sensitivities of 100 nm/RIU and 90 nm/RIU are comparable to those demonstrated in previous sensitivity sensors arrays exited in [23].

In this paper, we have performed a series of simulations wherein one of the resonators is filled with water and others are not. As demonstrated in Fig. 7, the black line represents all sensors are in air situation, while the red line is the case when one of sensors (H1-cavity-3) is subjected with water. It is important to note that only the resonant wavelength of sensor filled with water shifts and the other dips are unaffected. It can be confirmed that positive binding event occurs at any one of the sensors array since only their corresponding resonant wavelength would shift in the output spectra. The others show no shift of their resonant dips.

The detection limit of refractive index change (DL) is further researched which could be defined as [11,21]

$$\mathrm{DL} = \frac{\lambda}{SQ} \tag{2}$$

where λ is the resonant wavelength, S represents the refractive index sensitivity, and Q means the quality factor. The numerical simulations show that the detection limit of refractive index change is about 5.63×10^{-4}, which is well optimized than the previous design [21]. The DL is small enough for label-free detection in PhC sensor arrays.

In addition, we further discuss the crosstalk between each sensor unit based on the crosstalk calculation defined as [23]

$$\eta_{crosstalk} = 10\times\lg\frac{1-A_i}{1-A} \tag{3}$$

where A is the transmission minimum value of resonant dip of one sensor at the resonant frequency. A_i represents the transmission value of other adjacent sensors at the same frequency. The calculated crosstalk between cavity-3, cavity-4 and cavity-5 is lower than -13 dB which has predominance in the multiplexed sensing detection, much lower than -4 dB in [23].

4. Conclusion

In this paper we have proposed a novel nanoscale photonic crystal sensors array based on a two dimensional radius vertical graded PhC silicon slab. The radius vertical graded photonic crystal sensors array consists of five resonant cavities interlaced-coupled to a W1 waveguide with high Q factor and high transmittance. Each resonant wavelength dip can shift independently with crosstalk lower than -13 dB corresponding to a change in refractive index of the near field region surrounding the resonant cavity. The simulation results demonstrate that the refractive index sensitivity of this device can reach 100 nm/RIU, and the quality factor of the resonators near 10^4 has been achieved. Our results suggest a refractive index detection limit is around

5.63×10^{-4}. Besides, the small footprint of the device ($12.48 \times 7.20\ \mu m^2$) has a strong potential in on-chip biochemical sensing arrays. Further extending the device geometry along horizontal direction could allow an even larger degree of multiplexing on monolithic substrates, which is an inherent advantage of our design for optical integrated circuits.

Acknowledgment

This work was supported in part by the NSFC under Grant no. 61372038, the National 973 Program under Grant no. 2012CB315705, the NSFC under Grant no. 61431003, the Fund of the State Key Laboratory of Information Photonics and Optical Communications (Beijing University of Posts and Telecommunications) and the Fundamental Research Funds for the Central Universities, China.

References

[1] Y. Liu, H. Salemink, Photonic crystal-based all-optical on-chip sensor, Opt. Express 18 (18) (2012) 29912–29920.
[2] S.H. Kwon, T. Sünner, M. Kamp, A. Forchel, Optimization of photonic crystal cavity for chemical sensing, Opt. Express 16 (16) (2008) 11709–11717.
[3] M. Scullion, A. Falco, T. Krauss, Slotted photonic crystal cavities with integrated microfluidics for biosensing applications, Biosens. Bioelectron. 27 (1) (2011) 101–105.
[4] A. Falco, L. Faolain, T. Krauss, Chemical sensing in slotted photonic crystal heterostructure cavities, Appl. Phys. Lett. 94 (2009) 063503.
[5] X. Zhao, J. Tsai, H. Cai, X. Ji, J. Zhou, M. Bao, Y. Huang, D. Kwong, A. Liu, A nano-opto-mechanical pressure sensor via ring resonator, Opt. Express 20 (8) (2012) 8535–8542.
[6] B. Song, S. Noda, T. Asano, Y. Akahane, Ultra-high-Q photonic double-heterostructure nanocavity, Nat. Mater. 4 (2005) 207–210.
[7] A. Sharkawy, S. Shi, D.W. Prather, Heterostructure photonic crystals: theory and applications, Appl. Opt. 41 (34) (2002) 7245–7253.
[8] D. Yang, H. Tian, N. Wu, Y. Yang, Y. Ji, Nanoscale torsion-free photonic crystal pressure sensor with ultra-high sensitivity based on side-coupled piston-type microcavity, Sens. Actuators A – Phys. 199 (2013) 30–36.
[9] B.T. Tung, D.V. Dao, T. Ikeda, Y. Kanamori, K. Hane, Susumu Sugiyama, Investigation of strain sensing effect in modified single-defect photonic crystal nanocavity, Opt. Express 19 (9) (2011) 8821–8829.
[10] J.L. Dominguez-Juarez, G. Kozyreff, J. Martorell, Whispering gallery microresonators for second harmonic light generation from a low number of small molecules, Nat. Commun. 2 (254) (2011), Art. ID 254.
[11] Y. Yang, D. Yang, H. Tian, Y. Ji, Photonic crystal stress sensor with high sensitivity in double directions based on shoulder-coupled aslant nanocavity, Sens. Actuators A – Phys. 193 (2013) 149–154.
[12] S. Mandal, D. Erickson, Nanoscale optofluidic sensor arrays, Opt. Express 16 (3) (2008) 1623–1631.
[13] K.B. Gylfason, C.F. Carlborg, A. Kaźmierczak, F. Dortu, G. Stemme, On-chip temperature compensation in an integrated slot-waveguide ring resonator refractive index sensor array, Opt. Express 18 (4) (2010) 3226–3237.
[14] M. Iqbal, M.A. Gleeson, B. Spaugh, F. Tybor, L.C. Gunn, Label-free biosensor arrays based on silicon ring resonators and high-speed optical scanning instrumentation, IEEE J. Sel. Top. Quantums 16 (3) (2010) 654–661.
[15] S. Pal, E. Guillermain, R. Sriram, B. Miller, P. Fauchet, Silicon photonic crystal nanocavity-coupled waveguides for error-corrected optical biosensing, Biosens. Bioelectron. 26 (10) (2011) 4024–4031.
[16] K. Ren, X. Ren, Controlling light transport by using a graded photonic crystal, Appl. Opt. 50 (15) (2011) 2152–2157.
[17] K. Do, X. Roux, D. Marris-Morini, L. Vivien, E. Cassan, Experimental demonstration of light bending at optical frequencies using a non-homogenizable graded photonic crystal, Opt. Express 20 (4) (2012) 4776–4783.
[18] B. Vasić, G. Isić, R. Gajić, K. Hingerl, Controlling electromagnetic fields with graded photonic crystals in metamaterial regime, Opt. Express 18 (19) (2010) 20321–20333.
[19] F. Gaufillet, É. Akmansoy, Graded photonic crystals for graded index lens, Opt. Commun. 285 (10–11) (2012) 2638–2641.
[20] Q. Wu, J.M. Gibbons, W. Park, Graded negative index lens by photonic crystals, Opt. Express 16 (21) (2008) 16941–16949.
[21] Q. Liu, H. Tian, D. Yang, J. Zhou, Y. Yang, Y. Ji, Nanoscale radius-graded photonic crystal sensor arrays using interlaced and symmetrical resonant cavities for biosensing, Sens. Actuators A – Phys. 216 (2014) 223–230.
[22] S.H. Mirsadeghi, E. Schelew, J.F. Young, Photonic crystal slot-microcavity circuit implemented in silicon-on-insulator: high Q operation in solvent without undercutting, Appl. Phys. Lett. 102 (13) (2013) 131115.
[23] D. Yang, H. Tian, Y. Ji, Nanoscale low crosstalk photonic crystal integrated sensors array, IEEE Photonics J. 6 (1) (2014) 4200107.